

# Harnessing Vector Multi-pulsing Soliton Dynamics

S. V. Sergeev<sup>1\*</sup>, H. Khashi<sup>1</sup>, C. Mou<sup>2</sup>

<sup>1</sup> Aston Institute of Photonic Technologies, Aston University B4 7ET Birmingham, United Kingdom

<sup>2</sup> Key Lab of Specialty Fiber Optics and Optical Access Network, Shanghai University, Shanghai 200444, China

E-mail: s.sergeev@aston.ac.uk

## ABSTRACT

We demonstrate that mode-locked fiber laser polarization dynamics is characterized by switching between orthogonal states of polarization. We use injecting optical signal with a slowly evolving state of polarization to control the dwelling time nearby each state of polarization and so support regular rather than random switching between the quasi-equilibrium states.

**Keywords:** mode-locked laser, solitons, breather,

## 1. INTRODUCTION

The main challenge of manipulating the networks of coupled oscillators toward targeted collective patterns is the limited ability to conduct experiments with engineering (sensor and telecom) and biological (cortex, flocking birds) networks in a reasonably short time and under laboratory-controlled conditions [1]. The short pulse duration of hundred femtoseconds and repetition rates of tens–hundreds of megahertz make multimode mode-locked lasers (MLLs) a suitable model system for studying the synchronization-driven swarming in controllable laboratory conditions and short time scale of seconds [2-10]. The central concept underpinning the lasers' operation is the synchronization of longitudinal modes. The synchronization leads through short-range (covalent) and long-range (non-covalent) weak pulses' interactions toward swarming pulses into different soliton supramolecules [5-10]. The most effective approach for control is based on tailoring optoacoustic effects [6] and dispersive wave emission [5] by using the continuous wave (cw) signal injection that enables the self-assembly of large numbers of optical solitons into the supramolecular structures. However, there is a limited number of waveforms to be generated and a challenge for mapping the required soliton supramolecule vs the laser cavity parameters and the power of the injected signal. Also, the approach creates an obstacle to drawing meaningful insights on feasible approaches for controlling self-organization scenarios for systems beyond laser physics and engineering.

Our recent experimental data and theoretical analysis demonstrated that the mode-locked fiber laser presents a heteroclinic system where the laser's eigenstates – orthogonal states of polarization - are quasi-equilibrium points [3, 4, 9-11]. The heteroclinic orbit is a trajectory periodically evolving nearby the neighborhood of one of the orthogonal SOPs with further switching to the other SOP [3, 4, 9-11]. The dwelling time for the trajectory near each orthogonal state is adjustable with the help of the polarization controller for the pump wave [3, 4, 9-11]. As follows from the Shil'nikov theorem [12-14], the heteroclinic system produces a large number of attractors which are located near the heteroclinic orbit connecting the quasi-equilibrium states. Herein, for the first time, we demonstrate theoretically for Er-doped mode-locked fiber laser that the injected signal with the rotating state of polarization enables the selection of the attractor corresponding to the specific multi-pulsing dynamics.

## 2. VECTOR MODEL OF MODE-LOCKED FIBER LASER WITH THE INJECTED SIGNAL

For mapping the multi-soliton dynamics driven by the external optical signal, we used a vector model of Er-doped mode-locked fiber laser recently developed by Sergeev and co-workers [9]. The model describes the evolution of the state of polarization (SOP) of the lasing averaged over the pulse width driven by injected signal with periodically evolving orthogonal states of polarization:

$$E_x = a \cdot \cos(\Omega t + \phi_0), E_y = a \cdot \sin(\Omega t + \phi_0) \cdot \exp(i \cdot \Delta\phi) \quad (1)$$

Here  $a$  is the amplitude of the injected optical signal,  $\Omega$  is the frequency of oscillations, and  $\phi_0$  is the initial phase,  $\Delta\phi$  is the phase difference between the orthogonal SOPs. With taking into account Eq. (1), the equations for evolution of the complex amplitudes of the lasing field and population inversion can be presented as follows:

$$\begin{aligned} \frac{du}{dt} &= i\beta u + i\frac{\gamma}{2} \left( |u|^2 u + \frac{2}{3} |v|^2 u + \frac{1}{3} v^2 u^* \right) + D_{xx} u + D_{xy} v + E_x, \\ \frac{dv}{dt} &= -i\beta v + i\frac{\gamma}{2} \left( |v|^2 v + \frac{2}{3} |u|^2 v + \frac{1}{3} u^2 v^* \right) + D_{xy} u + D_{yy} v + E_y, \\ \frac{dn_0}{dt} &= \varepsilon \left[ I_p + 2R_{10} - \left( 1 + \frac{I_p}{2} + \chi R_{10} \right) n_0 - \chi R_{11} n_{12} - \chi n_{22} R_{12} \right], \end{aligned}$$

$$\begin{aligned}
\frac{dn_{12}}{dt} &= \varepsilon \left[ \frac{(1-\delta^2)I_p}{(1+\delta^2)2} + R_{11} - \left(1 + \frac{I_p}{2} + \chi R_{10}\right) n_{12} - \left(\frac{(1-\delta^2)I_p}{(1+\delta^2)2} + \chi R_{11}\right) \frac{n_0}{2} \right], \\
\frac{dn_{22}}{dt_s} &= \varepsilon \left[ R_{12} - \left(1 + \frac{I_p}{2} + \chi R_{10}\right) n_{22} - \chi R_{12} \frac{n_0}{2} \right], \\
R_{10} &= \frac{1}{(1+\Delta^2)} (|u|^2 + |v|^2), \quad R_{11} = \frac{1}{(1+\Delta^2)} (|u|^2 - |v|^2), \quad R_{12} = \frac{1}{(1+\Delta^2)} (uv^* + vu^*),
\end{aligned} \tag{2}$$

Coefficients  $D_{ij}$  are found as follows:

$$\begin{aligned}
D_{xx} &= \frac{\alpha_1(1-i\Delta)}{1+\Delta^2} (f_1 + f_2) - \alpha_2 + \ln \left(1 - \frac{\alpha_0}{1 + \alpha_s(|u|^2 + |v|^2)}\right), \\
D_{yy} &= \frac{\alpha_1(1-i\Delta)}{1+\Delta^2} (f_1 - f_2) - \alpha_2 + \ln \left(1 - \frac{\alpha_0}{1 + \alpha_s(|u|^2 + |v|^2)}\right), \quad D_{xy} = D_{yx} = \frac{\alpha_1(1-i\Delta)}{1+\Delta^2} f_3.
\end{aligned} \tag{3}$$

where:

$$f_1 = \left(\chi \frac{n_0}{2} - 1\right), \quad f_2 = \chi \frac{n_{12}}{2}, \quad f_3 = \chi \frac{n_{22}}{2}. \tag{4}$$

Here time  $t$  is normalized to the photon lifetime in the cavity  $\tau_p$ ,  $I_x = |u|^2$ ,  $I_y = |v|^2$ , are normalized to the saturation power  $I_{ss}$  and  $I_p$  is normalized to the saturation power  $I_{ps}$ ;  $\alpha_1$  the total absorption of erbium ions at the lasing wavelength;  $\alpha_2$  represents the normalized losses;  $\alpha_0$  and  $\alpha_s$  are parameters describing carbon nanotubes (CNT) saturable absorber;  $\delta$  is the ellipticity of the pump wave,  $\varepsilon = \tau_p/\tau_{Er}$  is the ratio of the photon lifetime in the cavity  $\tau_p$  to the lifetime of erbium ions at the first excited level  $\tau_{Er}$ ;  $\chi = (\sigma_a + \sigma_e)/\sigma_a$ , ( $\sigma_a$  and  $\sigma_e$  are absorption and emission cross-sections at the lasing wavelength);  $\Delta$  is the detuning of the lasing wavelength with respect to the maximum of the gain spectrum (normalized to the gain spectral width),  $\beta$  is the normalized linear birefringence strength ( $2\beta = 2\pi L_c/L_b$ ,  $L_b$  is the beat length and  $L_c$  is the cavity length). We use an approximation in Eqs. (2) that the dipole moments of the absorption and emission transitions for erbium-doped silica are located in the plane orthogonal to the direction of the light propagation [3, 4, 9-11].

To obtain results shown in Fig. 1, we used the following parameters: a1)-c4)  $\beta_L = \beta_C = 0$ ,  $\alpha_1 = 10.8$ ,  $\alpha_2 = 1$ ,  $\alpha_s = 10^{-3}$ ,  $\alpha_0 = 0.136$ ,  $\varepsilon = 10^{-5}$ ,  $\chi = 2.3$ ,  $\Omega = 2.5 \cdot 10^{-4}$ ,  $\phi_0 = \pi/4$ ,  $\Psi = \pi/2$ . Also, a1)-c1)  $\delta = 0.99$ ,  $a = 0$ ; a2)-c2)  $\delta = 0.92$ ,  $a = 0$ ; a3)-c3)  $\delta = 0.92$ ,  $a = 1$ ; a4)-c4)  $\delta = 0.92$ ,  $a = 1.5$ . To account for the output POC transformation caused by the patchcord connected to the polarimeter, we use the following 3D rotation matrix [15]:

$$\begin{aligned}
\begin{pmatrix} \tilde{S}_1 \\ \tilde{S}_2 \\ \tilde{S}_3 \\ \tilde{S}_0 \end{pmatrix} &= \begin{bmatrix} a_{11} & a_{12} & a_{13} & 0 \\ a_{21} & a_{22} & a_{23} & 0 \\ a_{31} & a_{32} & a_{33} & 0 \\ 0 & 0 & 0 & 1 \end{bmatrix} \begin{pmatrix} S_1 \\ S_2 \\ S_3 \\ S_0 \end{pmatrix}, \\
a_{11} &= \cos(\psi) \cos(\gamma), \quad a_{12} = \cos(\gamma) \sin(\alpha) \sin(\psi) - \cos(\alpha) \sin(\gamma), \\
a_{13} &= \cos(\alpha) \cos(\gamma) \sin(\psi) + \sin(\alpha) \sin(\gamma), \\
a_{21} &= \cos(\psi) \sin(\gamma), \quad a_{22} = \cos(\alpha) \cos(\gamma) + \sin(\alpha) \sin(\psi) \sin(\gamma), \\
a_{23} &= -\cos(\gamma) \sin(\alpha) + \sin(\psi) \sin(\gamma), \quad a_{31} = -\sin(\gamma), \quad a_{32} = \cos(\psi) \sin(\alpha), \\
a_{33} &= \cos(\alpha) \cos(\psi).
\end{aligned} \tag{5}$$

The dynamics in terms of the Stokes parameters was extracted from the results of numerical solution of Eqs. (2) as follows:

$$\begin{aligned}
S_0 &= |u|^2 + |v|^2, \quad S_1 = |u|^2 - |v|^2, \quad S_2 = u \cdot v^* + v \cdot u^*, \quad S_3 = -i \cdot (u \cdot v^* - v \cdot u^*), \\
s_i &= S_i / \sqrt{S_1^2 + S_2^2 + S_3^2}, \quad (i = 1, 2, 3)
\end{aligned} \tag{6}$$

The powers for the orthogonal  $x$ - and  $y$ - polarization components ( $I_x$ ,  $I_y$ ), the total power  $I$  and the phase difference  $\Delta\varphi$  can be found as follows:

$$I_x = |u|^2, \quad I_y = |v|^2, \quad S_3/S_2 = \tan(\Delta\varphi). \quad (7)$$

### 3. RESULTS AND DISCUSSION

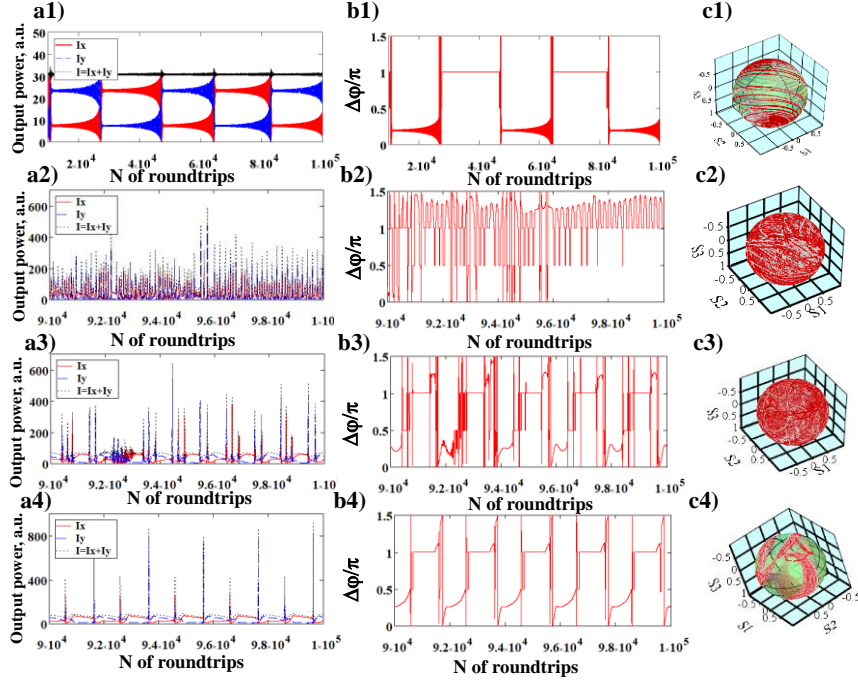


Figure 1. Polarization dynamics of multi-pulsing in terms of a1), a2), a3), a4): powers of individual polarization components  $I_x$  (red) and  $I_y$  (blue), the total output power  $I$ ; b1), b2) b3) b4): the phase difference  $\Delta\varphi$  between orthogonally polarized SOPs, and c1), c2) c3), c4): trajectories on Poincaré sphere.

As follows from Fig.1 (a1), when the pump wave ellipticity is close to one, and the injected signal is absent, e. g.  $\delta = 0.99, a = 0$ , dynamics takes the form of antiphase oscillations for  $x$  and  $y$  polarization components and so the constant total output power. Given that the model explores slow dynamics averaged over the pulse width, such dynamics means cw mode-locking with the periodic switching between two orthogonal elliptic SOPs and spiral attractor shown (Fig.1 b1 and c1). Due to the extreme sensitivity to the perturbations and according to the Shil'nikov theorem [18, 19], with decreased ellipticity, i. e.  $\delta = 0.92, a = 0$ , the spiral attractor is transformed into a hyperchaotic one, shown in Fig. 1 (c2). The hyperchaotic behavior takes the form of the random switching between the orthogonally polarized SOPs shown in Fig. 1 (a2 and b2). In the context of mode-locking, the random pulses in Fig. 1 (a2) are related to the slow dynamics, and so can comprise tenths of short pulses. With the injected signal, e. g.  $\delta = 0.92, a = 1$ , random pulses become sparser and more regular (Fig. 1 a3). Unlike the previous case, the phase difference in Fig. 1 (b3) has a longer duration of the time intervals with the constant value, which means dynamics with more extended synchronization between the orthogonal SOPs. Though trajectories on Poincaré sphere are not closed, they demonstrate more regular behavior (Fig. 1 c3). With a further increased amplitude of the injected signal to  $a = 1.5$ , the dynamics takes the form of regular pulses shown in Fig. 1 (a4). Because the duration of pulses is of tenths of roundtrips, such dynamics correspond to multi-pulsing. Regular dynamics is justified in Fig. 1 (b4), demonstrating the periodic switching between the orthogonal SOPs and in Fig. 1 (c4), showing polarization attractor with closed trajectories.

### 4. CONCLUSIONS

By using the vector model of Er-doped mode-locked fiber laser, we demonstrate theoretically that the injected signal with the rotating state of polarization enables control of the dwelling time nearby each orthogonal SOPs by adjusting its power, modulation frequency, and phase. As a result, mode-locking regimes take forms ranging from cw with switching between the orthogonal SOPs to chaotic (random multi-pulsing) and, finally, to periodic multi-pulsing. Beyond the fast manipulation of the optical waveforms for the controllable laser dynamics and encoding information in non-binary formats, the results can potentially unlock techniques for manipulating

synchronization and swarming in different biological, chemical and engineering systems with the heteroclinic dynamics.

## ACKNOWLEDGEMENTS

We acknowledge support from Leverhulme Trust grant HARVEST RPG-2023-073, UK EPSRC (EP/W002868/1), Horizon 2020 ETN MEFISTA (861152) and the National Natural Science Foundation of China grants: 61975107, 61605107 and the ‘111’ project grant D20031.

## REFERENCES

- [1] K. P. O’Keefe, H. Hong, and S. H. Strogatz: Oscillators that sync and swarm, *Nature Commun.*, vol. 8. p. 1504, Nov. 2017.
- [2] N. Akhmediev and A. Ankiewicz: Dissipative Solitons, Springer-Verlag, Berlin, Heidelberg, 2005.
- [3] S. V. Sergeyev, Fast and slowly evolving vector solitons in mode-locked fibre lasers, *Phil. Trans. R. Soc. A*, vol. 372. p. 20140006, Oct. 2014.
- [4] S. V. Sergeyev, *et. al.*: Spiral attractor created by vector solitons, *Light Sci. Appl.*, vol. 3. p. e131, Jan. 2014.
- [5] Z. Chang, *et. al.*: Real-time dynamics of optical controlling for bound states of mode-locked fiber laser with short-range interaction, *Opt. Laser Technol.*, vol. 149. p. 107859, May 2022.
- [6] W. He, *et. al.*: Formation of optical supramolecular structures in a fibre laser by tailoring long-range soliton interactions, *Nature Commun.*, vol. 10. p. 5756, Dec. 2019.
- [7] J. M. Dudley, F. Dias, M. Erkintalo, G. Genty: Instabilities, breathers and rogue waves in optics, *Nature Photon.*, vol. 8. pp. 755-764, Oct. 2014.
- [8] S. Chouli, P. Grelu: Rains of solitons in a fiber laser, *Opt. Express*, vol. 17. pp. 11776-11781, Jul. 2009.
- [9] S. V. Sergeyev, M. Eliwa, H. Khashi: Polarization attractors driven by vector soliton rain, *Opt. Express*, vol. 30. pp. 35663-35670, Sep. 2022.
- [10] S. Sergeyev, S. Kolpakov, Y. Loika: Vector harmonic mode-locking by acoustic resonance, *Photonics Res.*, vol. 9, pp. 1432-1438, Aug. 2021.
- [11] S. V. Sergeyev: Vector self-pulsing in erbium-doped fiber lasers, *Opt. Lett.*, vol. 41. pp. 4700-4703, Oct. 2016.
- [12] C. P. Silva, Shil’nikov’s theorem-a tutorial, *Circuits Syst. I. Fundam. Theory Appl.*, vol. 40. pp. 675-682, Oct. 1993.
- [13] G. Tigan, D. Opris: Analysis of a 3D chaotic system, *Chaos Solit. Fractals*, vol. 36. pp. 1315-1319, Jun. 2008.
- [14] I. M. Ovsyannikov, and L. P. Ovsyannikov: Systems with a homoclinic curve of multidimensional saddle-focus type, and spiral chaos, *Math. USSR Sb.*, vol. 73. p. 415, Feb. 1992.
- [15] D. A. Varshalovich, A. N. Moskalev, and V. K. Khersonskii: Quantum Theory of Angular Momentum, World Scientific, Singapore. pp. 21-23, 1988.